ELSEVIER

A fluid-pressure feedback model of dehydration reactions: experiments, modelling, and application to subduction zones

S.A. Miller[a,*], W. van der Zee[b], D.L. Olgaard[c], J.A.D. Connolly[a]

[a] Department of Earth Sciences, Geophysics Institute, ETH-Zurich, Zurich 8093, Switzerland
[b] Department of Geologie, RWTH, Aachen, Germany
[c] ExxonMobil Upstream Research Company, Houston, TX, USA

Abstract

Dehydration and melting reactions generate large volumes of fluid in the crust and upper mantle, and play an important role in subduction zone seismicity. The fluid pathway must evolve from isolated pockets in low porosity, low permeability rock, coalescing to interconnected permeable pathways to the surface. When fluid pressures generated from a dehydration or melting reaction are sufficient to induce hydrofracture, then hydrofracture significantly influences the porosity–permeability structure within the dehydrating/melting horizon. If a low fluid-pressure boundary is introduced to the dehydrating rock, then fluid will be driven from the rock along the evolved permeable network toward that boundary. The resulting pressure reduction can then accelerate the dehydration reaction and further drive the flow. The sudden introduction of a low fluid-pressure boundary may occur by the co-seismic (dilatant) rupturing of a pressure seal that connects different fluid pressure states. This mechanism is invoked to explain the observed post-seismic evolution of wave velocities (V_p/V_s) following the 1995 Antofagasta, Chile earthquake. We show experimental results and introduce a conceptual and numerical model that reflects this scenario. The model couples the mechanical and thermodynamic effects of fluid pressure with devolitization kinetics, and is quantitatively consistent with experimental studies of the dehydration of gypsum and serpentine. The experimental results show that dehydration is controlled by access to a free (drained) boundary. The model provides a mechanistic explanation for the experimental observations and has applications in understanding the role of transient transport networks on the large-scale behavior of dehydrating and melting systems.

1. Introduction

Large volumes of chemically bound fluids and volatile components are subducted, released, and recycled within the crust and upper mantle (Cathles, 1990; Peacock, 1990). Free fluids promote melting (Poli and Schmidt, 1995), deformation (Ko et al., 1997), and seismicity (Davies, 1999; Peacock, 2001). Current debate about the nature of fluid extraction from the crust centers around mechanisms for local veining and fracturing, and large-scale fluid channelling (Kelemen et al., 1997; Connolly and

* Corresponding author. Tel.: +41-1-633-2621; fax: +41-1-633-1065.
E-mail address: steve@erdw.ethz.ch (S.A. Miller).

Podladchikov, 1998). Ubiquitous evidence shows that fluid channelling is widespread, and that fluid flow in general is episodic from the continuous buildup and release of fluid overpressures (Walder and Nur, 1984; Cox, 1995). Fluid overpressures generated in dehydration reactions lead to weakening and embrittlement (Raleigh and Paterson, 1965; Rutter and Brodie, 1988) at the transition from isolated pores to interconnected pathways, and rheological and microstructural observations support the notion that fluid overpressures are common in dehydrating systems (Hubbert and Rubey, 1959; Ko et al., 1997). High-temperature anatectic melting experiments demonstrate that melting itself can generate hydrofracture (Connolly et al., 1997), with corresponding natural migmatite examples (Watt et al., 2000).

Dehydration reactions in subduction zones represent a substantial source of fluid and act as key component in the earthquake process (Kirby, 1995). Double seismic zones around subducting slabs are argued to result from serpentine dehydration on the upside of a down-going slab and mantle dehydration on the downside of the slab (Peacock, 2001). Seismically induced fluid flow following the 1995, $M_w = 8$ Antofagasta, Chile earthquake (Husen and Kissling, 2001) showed that the hydraulics of subduction change drastically over short time scales, and triggered by co-seismic rupturing of a pressure seal. Recent experimental evidence (Bons and van Milligan, 2001) shows that in fluid-producing systems, fluid flow is a self-organizing process where large fluxes occur over short time and length scales, and that ballistic (or cellular automaton) approaches to modelling are more appropriate than a continuum description for diffusion/advection systems.

Recent continuum modelling shows that porosity waves are a potentially important mechanism for fluid expulsion and channelling (Connolly and Podladchikov, 1998). If the viscous relaxation time is short, then porosity waves are the dominant process for fluid expulsion. Conversely, if the relaxation times are long, then hydrofracture is the likely mechanism for fluid transport. In general, continuum models ignore hydrofracture as a potentially important mechanism in crustal hydraulics, even though field evidence shows that hydrofracture is an important mechanism (Brown and Solar, 1998; Strating and Vissers, 1991). Stochastic models (Dagan, 1994) that assume a heterogeneous

permeability structure can reproduce flow patterns, but these models require a priori assumptions of the permeability network, thus limiting their utility for developing physical insight into the processes that govern the creation of permeable pathways. The importance of fluid pressures as a dominant mechanism for fracture formation and propagation is well documented (Walther and Wood, 1986; Fyfe et al., 1978). Evidence for hydrofracture exists at all levels of the crust and upper mantle, but few models have addressed on this mechanism. Nishiyama (1989) coupled kinetics with fracture mechanics to show that hydrofracture was both possible and likely in the antigorite dehydration reaction. Using percolation theory, he estimated that most hydrofracturing would occur early in the dehydration process, thus establishing a permeable network for flow of the remaining fluid generated from additional heat input. This is consistent with other modelling (Miller and Nur, 2000) that shows hydrofracture-controlled systems will naturally self-organize to a percolation threshold. A model that couples fluid expansion with fracture mechanics (Dutrow and Norton, 1995) demonstrated a possible mechanism for fluid pressure cycling during metamorphism.

The focus of this paper is to investigate the feedback of reaction and fracture in phase transitions (Chizhik and Sidelnikov, 1998; Ague et al., 1998; Simpson, 1999). We present a conceptual framework for incorporating crustal hydraulics into the dehydration process, and propose that rapid fluid pressure changes may significantly influence the dehydration process. Experimental and modelling results demonstrate the proposed processes.

2. Conceptual model

The prevailing view in subduction zones is that dehydration reactions play a substantial role in seismicity. A majority of previous studies focussed on constraining isotherms in subduction zones and constraining the pressure of the fluid at the rock pressure. However, earthquakes promote large changes in crustal hydraulics through co-seismic permeability enhancement (Sibson, 1992; Rojstaczer and Wolf, 1992; Rojstaczer et al., 1995), and changes in the volumetric strain field (Muir-Wood and King, 1993)

surrounding the rupture. These changes establish (potentially significant) pore pressure gradients, thereby rapidly changing the pore pressure state. This is shown in the conceptual model (Fig. 1), which applies to any dehydration or melting reaction with a positive Clapeyron slope. A positive slope in $P-T$ space implies that the volume of the fluid produced is greater than the porosity created by the reaction, thereby producing fluid overpressures (Hacker, 1997). Fluid overpressures generated from isolated reaction nuclei can induce local hydrofracture that

creates a small-scale permeable crack network (A). The increase in porosity and associated fluid pressure reduction can stimulate additional reaction because reaction kinetics depend both on the temperature and the pressure of the fluid. If the generated fluid pressures are again sufficient to induce hydrofracture, then the internal permeability network expands (B). In the absence of a drained boundary or other mechanisms for reducing fluid pressures, the system is buffered and additional heat input is required for the reaction to continue. When a drained boundary, or
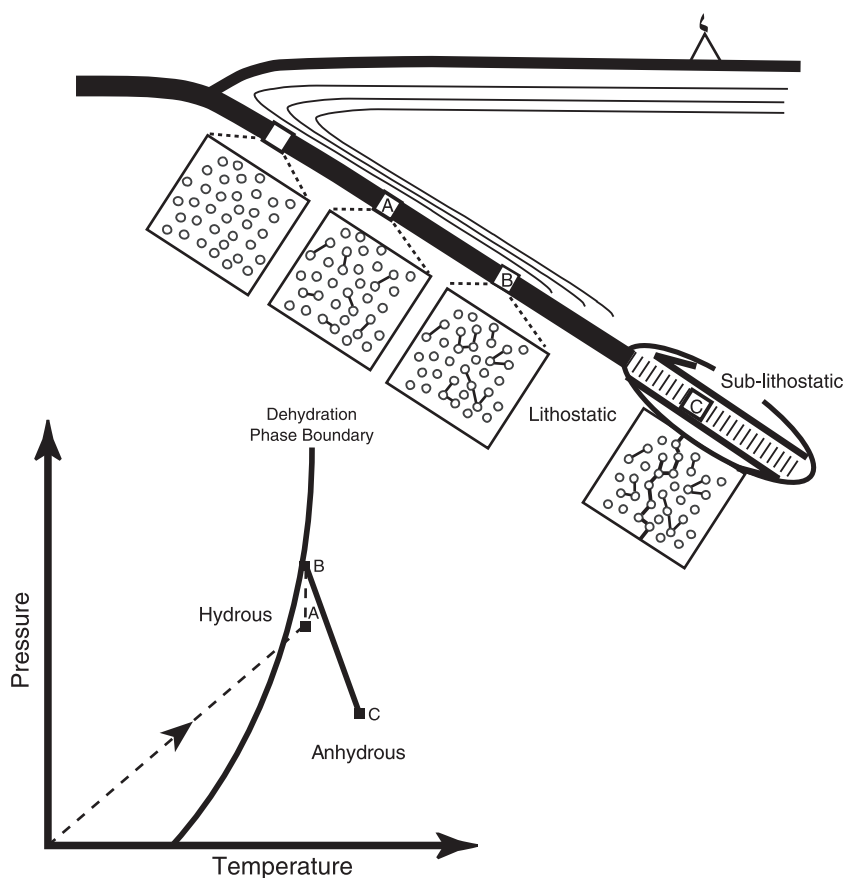

Fig. 1. Conceptual framework for a fluid pressure-controlled dehydration model in subduction zones. Under conditions of increasing temperature and pressure, dehydration reactions begin for certain minerals (A), resulting in an overpressure when the volume of the reaction products is greater than the porosity created by the reaction. Two consequences may follow: (1) the pressure increase buffers the reaction and the reaction ceases until additional thermal energy is input to the system (B); or (2) fluid pressure is sufficient to initiate a hydrofracture. If hydrofracture occurs, the fluid pressure is reduced from the increase in crack porosity or hydraulic communication with a low-pressure region, thus driving the state of the rock deeper into the stability field of the anhydrous assemblage and locally accelerating the reaction (C). A large earthquake will rupture the seal separating near-lithostatic fluid pressures and sub-lithostatic fluid pressures, thus promoting further reaction (see also Husen and Kissling, 2001). Fluid will escape the system by a route determined by the evolution of dehydration-induced connected network, and fluid flow into the overlying lithosphere can promote melting.

connectivity to a low-pressure region is present (C), fluid pressure reduction accelerates the reaction at all locations connected to it, and fluid will flow along the permeable channels developed during its evolution. The interplay between the growth of local to percolated networks leads to focused fluid expulsion. In subduction zones, if high fluid pressure is trapped behind a seal, then co-seismic rupturing of the seal will induce fluid flow if it then connects with sublithostatically pressured fluids (Fig. 1). This is the proposed explanation for spatio-temporal changes in V_p/V_s ratios observed following the Antofagasta, Chile earthquake (Husen and Kissling, 2001). Husen and Kissling observed high ratios of seismic velocity that correlated with the subducting Nazca plate directly above the plate interface, and with the regions of highest slip. They attributed this observation to co- and post-seismic fluid flow initiated by the earthquake. Near-lithostatic fluid pressures at the time of an earthquake has been demonstrated (Miller, 2002), and if co-seismic rupturing of a seal occurs, then large-scale fluid flow results. Kinetically, reduced fluid pressure drives the system further into the field of the anhydrous phase and devolitization accelerates. The effect of an earthquake on kinetics is even more enhanced if significant frictional heat is generated by the slip event.

To demonstrate this process, we present experimental results and results of a simple model that couples evolving fluid pressure with dehydration kinetics.

3. Experimental results

We present experimental results of dehydration experiments from two different rock types, alabaster gypsum from Volterra, Italy (Ko et al., 1997), and antigorite serpentinite from Val Malenco, Italy. The first reaction considered (gypsum $\rightarrow$ bassanite + $H_2O \rightarrow$ anhydrite) has been previously studied in the context of dehydration-induced weakening and embrittlement (Ko et al., 1997; Heard and Rubey, 1966; Wong et al., 1997). The phase transition from gypsum to the metastable phase bassanite produces about 37% H_2O and a solid volume reduction about 30% (net excess fluid volume $\approx$ 7%). The gypsum had an initial porosity of 0.5%, and an initial permeability

of 5×10^{-21} m^2 (Wong et al., 1997). The second dehydration process considered is the reaction (antigorite $\rightarrow$ olivine + talc + $H_2O \rightarrow$ enstatite + forsterite + H_2O). This reaction produces about 25% H_2O (Nishiyama, 1989; Wong et al., 1997). The starting material for these experiments was primarily antigorite with minor amounts of chlorite and brucite. The experimental configuration (Fig. 2) consisted of a jacketed sample subjected to a confining stress and a constant temperature boundary applied along the sample length. The specimens were jacketed in polyolifin (gypsum) or iron (serpentine) with an impermeable cap on one end, and a permeable cap on the drained end. The gypsum experiments were performed at 110 °C (heated at 10 °C/min until experimental temperatures were reached), a confining pressure of 60 MPa, and pore pressures were maintained at 10 MPa. The serpentine experiments were performed at 700 °C, where temperatures were increased to 500 °C at 10 °C/min under confining and pore pressures of 200 and 100 MPa, respectively. The confining and pore pressure were increased and maintained to 300 and 200 MPa, respectively, while the experimental temperature of 700 °C was reached, again at 10 °C/min. In each experiment, the volume of the expelled fluid was measured via an automated volumometer, set to maintain a constant pore pressure as exsolved fluids drained through the end of the sample under the applied pressure and temperature conditions.

The three experiments on gypsum were halted at different stages of the reaction to establish the evolution of reaction within the sample interior (Fig. 2a, I–III). Specimens from each stage were sectioned and imaged with backscatter scanning electron microscopy (SEM) to determine the spatial distribution of bassanite. Early in the reaction (I), bassanite reaction products are limited to the region of the drained boundary. As the reaction progresses (II), reaction products appear as clusters along the drained boundary and within the sample interior. No reaction products are observed at the undrained end. At later times (III), reaction products are uniformly distributed within the sample. These results demonstrate the reaction progresses from the drained boundary into the specimen interior, and the observed microstructure relates to the measured fluid expulsion (discussed below).

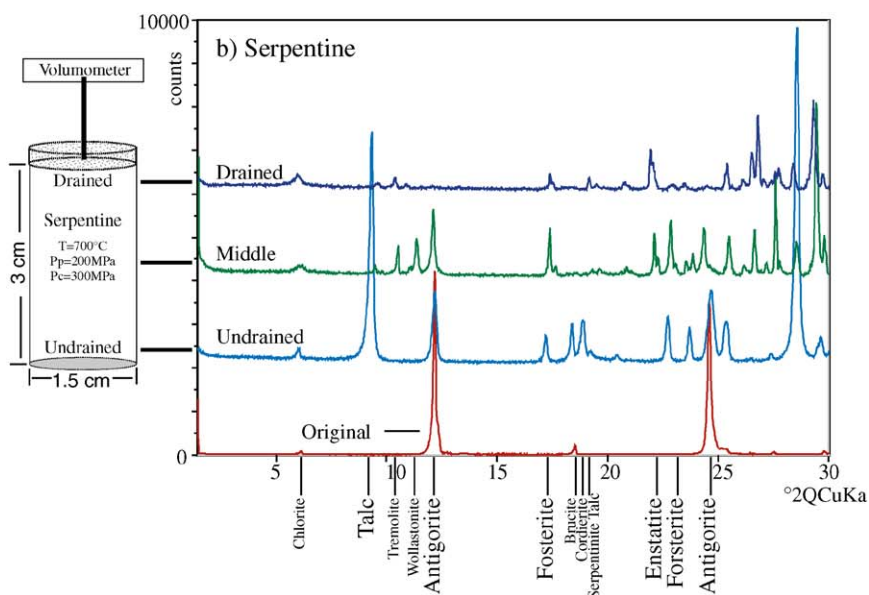Serpentine dehydration results in many different minerals, so analysis of the serpentine experiments
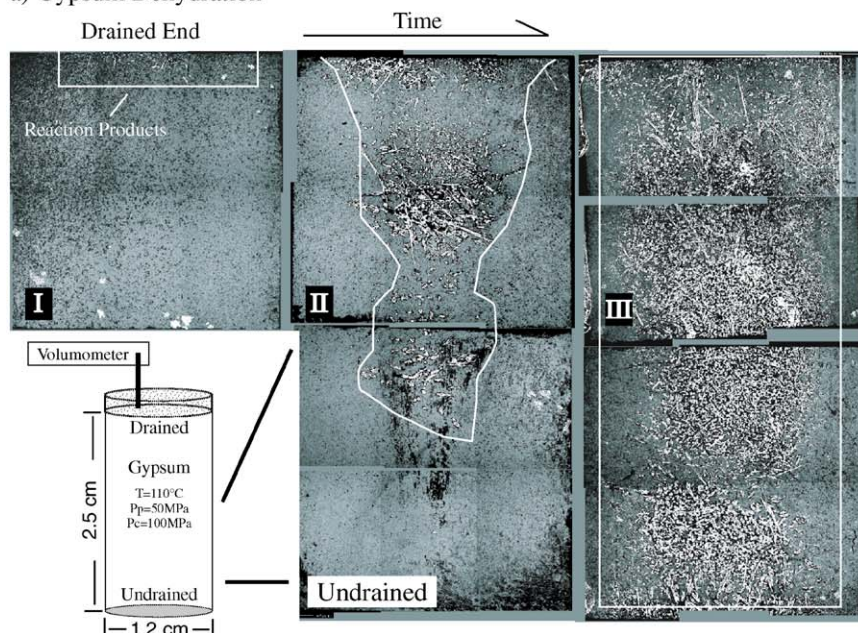
Fig. 2. Experimental results of (a) gypsum and (b) serpentine dehydration. In the early stages of gypsum dehydration (a), reaction products are limited to minor amounts at the drained end of the sample, and no reaction bassanite is observed within the sample interior (I). As the reaction progresses (II), the reaction products are concentrated around the drained end and a cluster of reaction products is observed in the sample interior. At this stage, no reaction products are observed at the undrained end. Note: A minor temperature difference of about 2 °C in the experimental cell went from higher temperature at the undrained end to lower temperature at the drained end, opposite to that of arguments for temperature-induced differential dehydration. With additional reaction (III), reaction products are observed throughout the specimen. In serpentine (b), XRD results show complete antigorite dehydration at the drained boundary, while at the undrained end, the original antigorite was still transforming to talc and forsterite. The central section is shown in a state between these two extremes.

was done by X-ray diffraction to unambiguously identify the different phases. Sections were cut from the drained, middle, and undrained portions of the test specimen (Fig. 2b). The X-ray diffraction analysis shows the composition of the original starting material and then, successively, the undrained, middle, and drained end portions of the specimen. In the undrained end, metastable talc is present with some of the original antigorite, indicating the initial stages of reaction. In the middle section, most of the original antigorite is gone, and the talc has transformed to enstatite and forsterite. In the section adjacent to the drained boundary, the reaction has gone to completion producing orthopyroxene and olivine. Therefore, the experimental results from two different rock types demonstrate that the dehydration reaction is rock-type independent, and is controlled by access to the low-pressure boundary. Both experiments show that the dehydration front propagates from the drained boundary, and the degree of reaction progress is a function of distance (or access) to this boundary.

A physical explanation for the experimental observations in the context of our model can be expressed in terms of the following sequence. Reaction in the sample interior generates significant overpressures in the neighborhood of dehydration nuclei for low porosity, low permeability rock. If the nuclei are far from the drained boundary, then they are not influenced this boundary, and either (i) the reaction is buffered by the excess pore pressures, or (ii) small-scale hydrofracture occurs and pressures equilibrate locally at a lower fluid pressure and the reaction continues. If the reaction occurs near the drained end, the fluid is expelled and the fluid pressure reduces to the drained fluid pressure. Lower fluid pressure accelerates reaction to completion and establishes a high-permeability channel. With additional time, the local permeability networks generated in the sample interior link with the boundary propagating into the sample interior. At late times, the internal permeability network is sufficiently mature such that connectivity to the boundary drains a large part of the sample, thus accelerating reaction and fluid expulsion. The channels that develop can there-

fore expel large volumes of fluid through very narrow channels because of the interconnected pathway.

4. The numerical model

A numerical model, based on the concepts in Fig. 1, couples reaction rate and fluid pressure for the dehydration reaction Chl + Mu = Bio + Qz + And/Ky + H$_2$O (Chl = chlorite, Mu = muscovite, Bio = biotite, Qz = quartz, And = andalusite, and Ky = kyanite). We choose this reaction because it is a potentially important metamorphic water source in pelitic rocks and its kinetics are plausibly constrained by analogy with experimentally studied reactions (Connolly, 1997; Lasaga and Rye, 1993). The kinetics of this reaction are used to determine the fluid production rates in a simple cellular automaton model of fluid pressure evolution (see details of the model in Miller and Nur, 2000).

The computational matrix of 200×200 cells contains a normal distribution of mineralogical heterogeneity described by perturbations (ΔH) about a mean enthalpy of reaction δH. The change in the Gibbs free energy (ΔG) of the reaction is calculated:

$$\Delta G = \Delta H \pm P\Delta V_s + T\Delta S + \upsilon_{H_2O}RT\ln f_{H_2O} \qquad (1)$$

where ΔH is the noise component of the enthalpy, P is the fluid pressure, V_s the solid volume, S is the entropy, υ is the stoichiometry coefficient for water, R is the gas constant, and f_{H_2O} is the water fugacity. The rate of fluid production ($\dot{\Gamma}$) and porosity creation ($\dot{\phi}$) are calculated as a function of ΔG and the percent reaction is monitored. During a time step Δt, the fluid pressure in cell i for a no-flow condition is
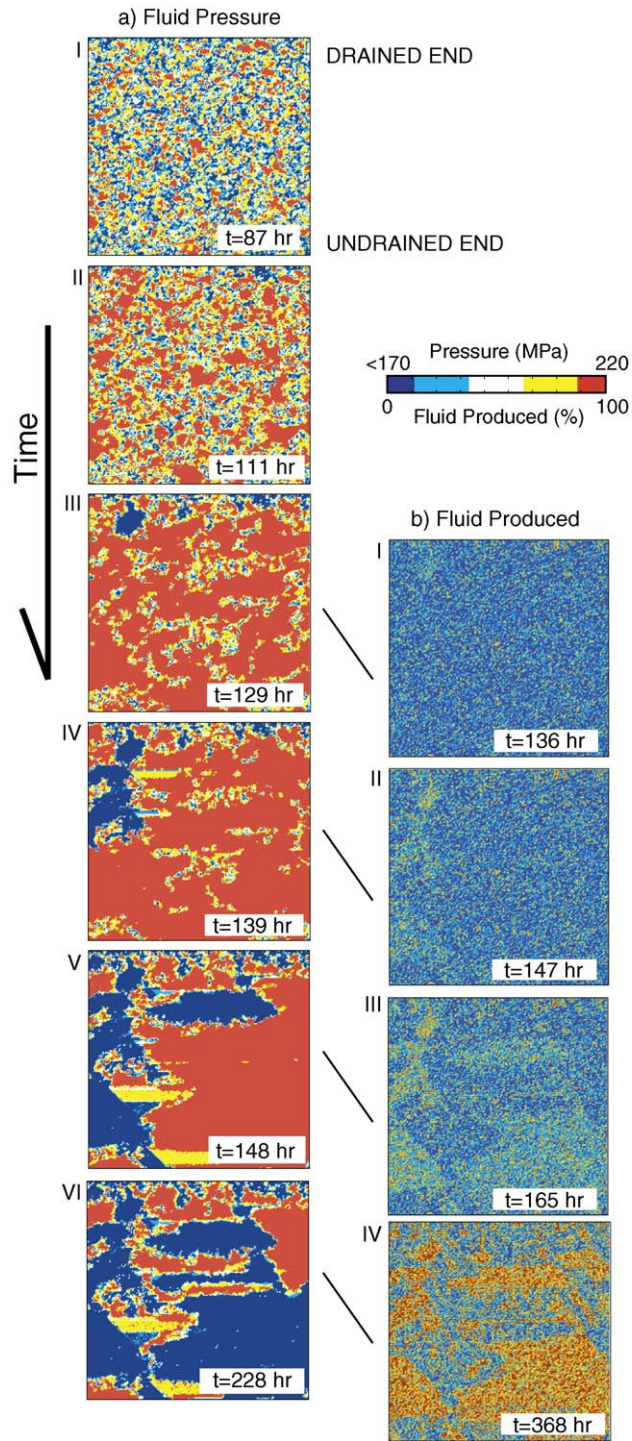
$$P_i(t + \Delta t) = P_i(t) + r_i(\Delta t) \qquad (2)$$

where

$$r_i = \frac{(\dot{\Gamma}(P, T) - \dot{\phi}(P, T))_i}{(\phi\beta)_i} \qquad (3)$$

The compressibility β includes pore and fluid compressibility and ranges from $1 \times 10^{-3} < \beta < 1 \times 10^{-2}$

Fig. 3. The evolution of fluid pressures in the model show isolated zones of fluid overpressure at early times (I), coalescing to a complex pressure state (II). As the model evolves, some regions begin to connect to the drained boundary (III), while internal networks continue to grow and coalesce (IV–V). At late times (VI), most of the numerical sample is connected to the drained boundary, and the reaction accelerates. (b) The corresponding fluid production shows how connectivity to the boundary accelerates the reaction (quantified in Fig. 4).

a) Fluid Pressure

DRAINED END

UNDRAINED END

Pressure (MPa)
<170   220

0   100
Fluid Produced (%)

b) Fluid Produced

Time

MPa^{-1} (David et al., 1994; Segall and Rice, 1995). We assume an initial porosity (ϕ) of 1%, a confining stress of 200 MPa, a constant temperature of 680 °C, and a drained boundary pressure of 30 MPa. Temperature changes associated with the endothermic reaction are currently ignored. If the fluid pressure generated during a time step is sufficient to meet the failure condition, then hydrofracture is assumed to occur and fluid pressure is redistributed locally (e.g. nearest neighbor cells) by conserving fluid mass. The failure condition is set at 10% above the confining pressure to approximate fracture toughness. More realistic fracture models (e.g. Simpson, 1999), or including stress changes induced by an opening mode dislocation (e.g. Okada, 1992) would significantly improve this model, but this is deferred to future developments. Permeability is treated as a toggle switch (Miller and Nur, 2000), with zero permeability before hydrofracture and infinite permeability to neighbor cells at hydrofracture. Experimental studies show that this is a reasonable approximation to flow in fluid-producing systems (Bons and van Milligan, 2001).

Flow is restricted to a cell until reaction-enhanced fluid pressures reach the failure threshold where a local crack network (e.g. nearest neighbors) is created. If the pressure of the affected cells remains above the failure condition, then the high fluid pressure propagates until all cells are below the failure condition. Connectivity to the free surface is monitored. If a cell at the drained boundary reaches the failure condition, it is identified and remains at the drained fluid pressure with ongoing reaction. When a neighbor to a boundary-connected cell communicates with that cell, it too becomes connected to the drained boundary. The basic behavior of the model, without direct coupling to reaction kinetics, shows the evolution to power law statistics of cluster sizes at and beyond the percolation threshold (Miller and Nur, 2000), implying a fractal geometry of connected pathways and in good agreement with observations (Clark et al., 1995).

5. Results

The evolution of internal fluid pressure is controlled by reaction kinetics (Fig. 3a). At early times (I–II), locally connected networks of overpressure begin to emerge. These regions represent areas of low effective confining stress, and so would tend slip given a low differential stress (e.g. mechanical weakening). Undrained experiments show that such mechanical occurs even after minor amounts of reaction (Olgaard et al., 1995). In transiently drained experiments (Ko et al., 1997), it was shown that if the permeability network grows uniformly, fluid drainage inhibits weakening. As the system evolves (III–IV), channels form as connectivity to the drained cells empties areas in the computational matrix that have already evolved to an interconnected network. Regions that remain undrained (V–VI) continue to interconnect and the permeable network grows. This results in a large region of fluid overpressure that ultimately requires only one connected cell to drain the entire hydraulically connected zone. The link between a large region of hydraulically connected fluid and the free boundary demonstrates fluid channelling as direct consequence of this model. Associated fluid production (Fig. 3b, I) shows that some reaction has occurred near the drained boundary (see also Fig. 2a), but little reaction has occurred in the sample interior because of the buffering effect of high fluid pressures. Drainage of these areas then spurs reaction (Fig. 3b, II; Fig. 2a). When the large internal network links with the low-pressure boundary, the entire connected region becomes under-pressured and accelerates the net reaction rate. Connectivity to the drained boundary produces a complex boundary structure that evolves to a thorough-going channel. This result implies that the macroscopic distribution of reaction products can appear relatively homogeneous, while fluid channelling is very localized with large fluid fluxes along limited flow paths. Additional fluid produced within the body would follow this defined channel to the drained boundary. The geometry of the channel is determined by its evolution. That is, the channel appears because of the linking of numerous isolated networks scattered through the body, and these networks are controlled by the kinetic and fracture properties of the rock.

A comparison of measured and modelled fluid expulsion (Fig. 4) shows that the model captures the dominant aspects of the experimental results. (We assume that fluid production in the model is a proxy for fluid expulsion because it includes connectivity to the drained boundary and is associated with high-permeability channels.) Both the experiments and the
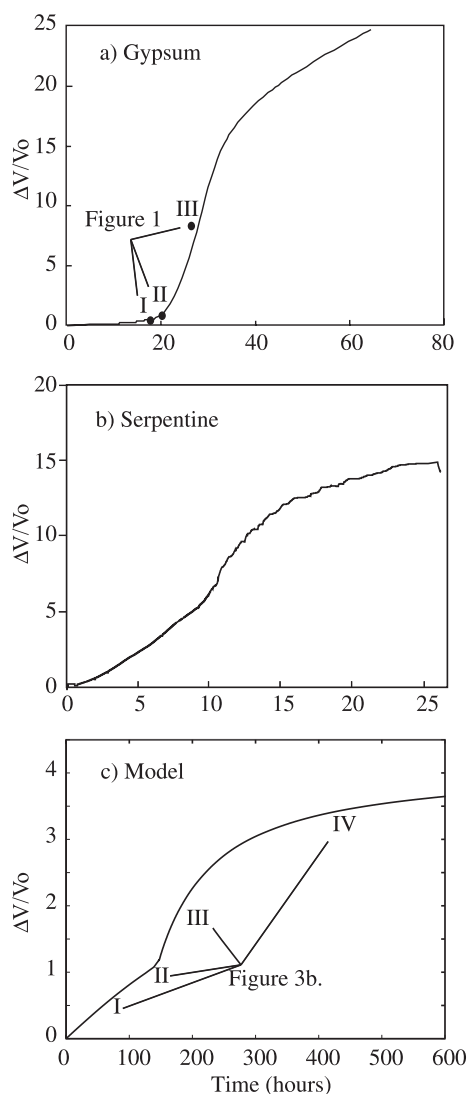
Fig. 4. Comparison of experiment and model fluid expulsion. Panel a corresponds to Fig. 2a, panel b to Fig. 2b, and panel c to Fig. 3b.

6. Discussion and conclusions

Experiments and modelling show that dehydration reactions can generate a permeable microcrack network, created by the self-organization of hydraulic connectivity from the fluid-filled porosity produced by individual reaction nuclei. The evolution of the internal permeable network is controlled by a feedback loop in which pressure reductions associated with crack-enhanced porosity have the same kinetic effect on dehydration as an increase in temperature. As the system evolves, fluid overpressures impede additional reaction until communication of these fluid pressure pockets with a low fluid-pressure boundary. The complex permeable network established within the body thus determines the degree of fluid expulsion (through channels) when ultimate connectivity to the boundary is achieved. These channels act as low-pressure pressure fronts that propagate into the sample interior, drain sub-networks of evolved hydraulically connected regions, and promote reaction. The model successfully reproduces the observed dehydration reaction front and fluid expulsion curves. The model has broad implications about the mechanisms of fluid extraction and expulsion in the earth's crust. Model results suggest that local interactions and permeability evolution from dehydration reactions tend to self-organize to a percolation-type threshold of interconnected regions. In the vicinity of a drain (for example, after a large earthquake and associated large fluid pressure perturbations), the rapid fluid pressure reduction can spur additional reaction and contribute to mechanisms of channelling of metamorphic fluids. In this model, it is the nucleation, growth, and coalescence of small-scale permeable networks that control the system evolution, so large-scale fractures are not necessary for channelling and localized fluid expulsion. The model may also apply to melting reactions and melt migration, where the melt overpressures are sufficient to induce local hydrofracture.

Modelling results are recast into a proposed process in subduction zones (Fig. 5). In this scenario, a pressure seal isolates the hydraulics of the subducting slab from the overlying lithosphere. With the seal intact, the fluid pressure generated by dehydration can establish an internally permeable network by the nucleation, growth, and coalescence of reaction-in-

model show relatively limited fluid expulsion followed by an acceleration of fluid expulsion rate as interior regions link with the evolving boundary. We interpret the increased fluid expulsion rate as marking a percolation threshold within the rock and the consequent acceleration of the reaction in response to the reduction in fluid pressure. An alternative explanation is related to the high permeability achieved by the reaction-induced porosity increase, with accelerated fluid expulsion driven by compaction (Wong et al., 1997).
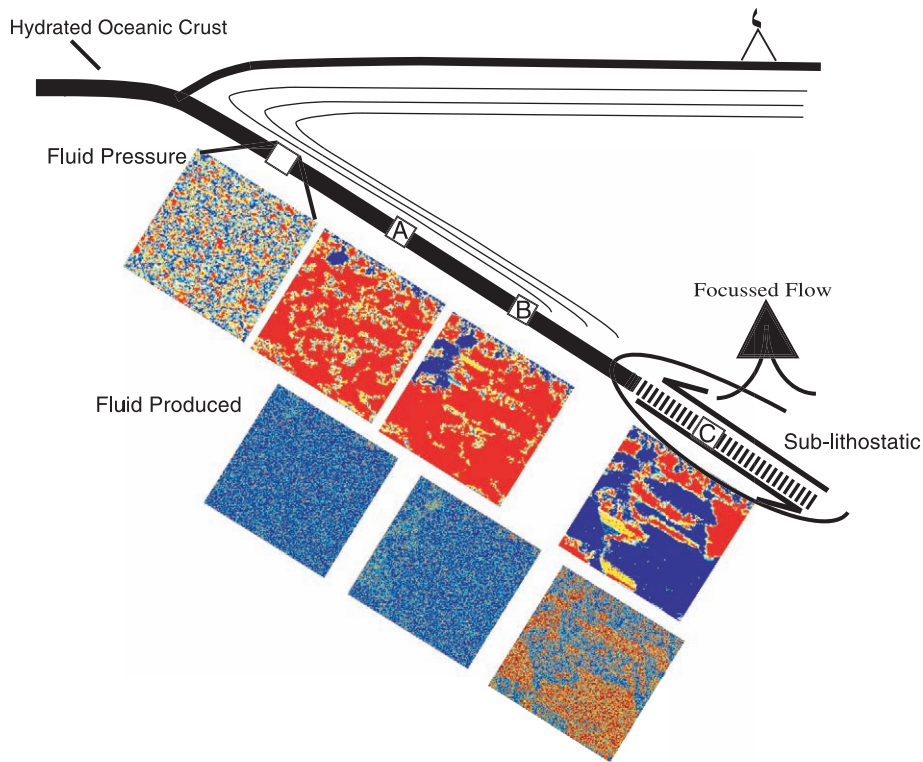
Fig. 5. Model results superposed on the conceptual model in Fig. 1. The colored figures show model results of a fluid pressure-controlled model for dehydration reactions where dehydration kinetics are coupled to a simple model for crustal hydraulics that treats permeability as a toggle switch. The top frames show the evolution of fluid pressure (blue is low) assuming a drained boundary on the upper end, and the lower frames show the subsequent fluid produced by the pressure reduction. Dehydration of the slab provides an important fluid source to drive earthquake-induced flow.

duced hydrofractures. At the time of a large subduction zone earthquake at depths where dehydration reactions are active, fluid pressure can be drastically reduced by the simultaneous rupture of the seal and dilatant slip. The fluid pressure reduction, combined with frictional heating, accelerates the reaction and drives the flow. This scenario is consistent with the interpretation of observed spatio-temporal variations in V_p/V_s following the 1995 $M_w = 8.0$ Antofagasta, Chile subduction zone earthquake (Husen and Kissling, 2001).

Acknowledgements

We thank J. Chery and B. Evans for reviews, and the XRD analyses of R. Neutsch are gratefully

References

Ague, J., Park, J., Rye, D., 1998. Regional metamorphic dehydration and seismic hazard. Geophys. Res. Lett. 22, 4224–4421.

Bons, P., van Milligan, B., 2001. New experiment to model self-organized critical transport and accumulation of melt and hydrocarbons from their source rocks. Geology 29, 919–922.

Brown, M., Solar, G., 1998. Shear zone systems and melts: feedback relations and self-organization in orogenic belts. J. Struct. Geol. 20, 211–227.

Cathles, L., 1990. Scales and effects of fluid flow in the upper crust. Science 248, 323–328.

Chizhik, S., Sidelnikov, A., 1998. Kinetics of solid state reactions with a positive feedback between reaction and fracture: 2. The kinetics of ion exchange in an alkaline-silicate glass. Russ. Chem. Bull. 47, 610–614.

Clark, M., Brantley, S., Fisher, D., 1995. Power-law vein thickness distributions and positive feedback in vein growth. Geology 23, 975–978.

Connolly, J., 1997. Devolatization-generated fluid pressure and deformation-propagated fluid flow during prograde regional metamorphism. J. Geophys. Res. 102, 18149–18173.

Connolly, J., Podladchikov, Y., 1998. Compaction-driven fluid flow in viscoelastic rock. Geodin. Acta 11, 55–84.

Connolly, J., Holness, M., Rubie, D., Rushmer, T., 1997. Reaction-induced microcracking: an experimental investigation of a mechanism for enhancing anatectic melt extraction. Geology 25, 591–594.

Cox, S., 1995. Faulting processes at high fluid pressures: an example of fault valve behavior from the Wattle Gully Fault, Victoria, Australia. J. Geophys. Res. 100, 12841–12859.

Dagan, G., 1994. The significance of heterogeneity of evolving scales of transport in porous formations. Water Resour. Res. 30, 3327–3336.

David, C., Wong, T.-F., Zhu, W., Zhang, J., 1994. Laboratory measurement of compaction-induced permeability change in porous rocks: implications for the generation and maintenance of pore pressure excess in the crust. Pure Appl. Geophys. 143, 425–456.

Davies, J., 1999. The role of hydraulic fractures and intermediate-depth earthquakes in generating subduction-zone magmatism. Nature 398, 142–145.

Dutrow, B., Norton, D., 1995. Evolution of fluid pressure and fracture propagation during contact metamorphism. J. Metamorph. Geol. 13, 677–686.

Fyfe, W., Price, N., Thompson, A., 1978. Fluids in the Earth's crust. Elsevier, Amsterdam.

Hacker, B., 1997. Diagenesis and fault valve seismicity of crustal faults. J. Geophys. Res. 102, 24459–24467.

Heard, H., Rubey, W., 1966. Tectonic implications of gypsum dehydration. Geol. Soc. Amer. Bull. 77, 741–760.

Hubbert, M., Rubey, W., 1959. Role of fluid pressure in the mechanics of overthrust faulting. Geol. Soc. Amer. Bull. 70, 115–166.

Husen, S., Kissling, E., 2001. Postseismic fluid flow after the large subduction earthquake of Antofagasta, Chile. Geology 29, 847–850.

Kelemen, P., Hirth, G., Shimizu, N., Spiegelman, M., Dick, H., 1997. A review of melt migration processes in the adiabatically upwelling mantle beneath oceanic spreading ridges. Philos. Trans. R. Soc., A 355, 283–318.

Kirby, S., 1995. Intraslab earthquakes and phase changes in subducting lithosphere. Rev. Geophys., 287–297 (supp., Report to International Union of Geodesy and Geophysics).

Ko, S.-C., Olgaard, D., Wong, T.-F., 1997. Generation and maintenance of pore pressure excess in a dehydrating system: 1. Experimental and microstructural observations. J. Geophys. Res. 102, 825–839.

Lasaga, A., Rye, D., 1993. Fluid flow and chemical reaction kinetics in metamorphic systems. Am. J. Sci. 293, 361–404.

Miller, S., 2002. Earthquake scaling and the strength of seismogenic faults. Geophys. Res. Lett. 29, 10.1029/2001GL014181.

Miller, S., Nur, A., 2000. Permeability as a toggle-switch in fluid-controlled crustal processes. Earth Planet. Sci. Lett. 183, 133–146.

Muir-Wood, R., King, G., 1993. Hydrological signature of earthquake strain. J. Geophys. Res. 98, 22035–22068.

Nishiyama, T., 1989. Kinetics of hydrofracturing and metamorphic veining. Geology 17, 1068–1072.

Okada, Y., 1992. Internal deformation due to shear and tensile faults in a half-space. Bull. Seismol. Soc. Am. 82, 1018–1040.

Olgaard, D., Bruhn, D., Miller, S., 1995. An assessment of experimental data on the mechanical properties of continental and oceanic rocks. Tech. Rep. 940392, ETH-Zurich.

Peacock, S., 1990. Fluid processes in subduction zones. Science 248, 329–337.

Peacock, S., 2001. Are the lower planes of double couple seismic zones caused by serpentine dehydration in subducting oceanic mantle? Geology 29, 299–302.

Poli, S., Schmidt, M., 1995. H_2O transport and release in subduction zones: experimental constraints on basaltic and andesitic systems. J. Geophys. Res. 100, 22299–22314.

Raleigh, C., Paterson, M., 1965. Experimental deformation of serpentinite and its tectonic implications. J. Geophys. Res. 70, 3965–3985.

Rojstaczer, S., Wolf, S., 1992. Permeability changes associated with large earthquakes: an example from Loma Prieta, California. Geology 20, 211–214.

Rojstaczer, S., Wolf, S., Michel, R., 1995. Permeability enhancement in the shallow crust as a cause of earthquake-induced hydrological changes. Nature 373, 237–238.

Rutter, E., Brodie, K., 1988. Experimental "syntectonic" dehydration of serpentenite under conditions of controlled pore water pressure. J. Geophys. Res. 93 (B5), 4907–4932.

Segall, P., Rice, J., 1995. Dilatancy, compaction, and slip instability of a fluid infiltrated fault. J. Geophys. Res. 100, 22155–22171.

Sibson, R., 1992. Implications of fault-valve behavior for rupture nucleation and recurrence. Tectonophysics 211, 283–293.

Simpson, G., 1999. Evolution of strength and hydraulic connectivity during dehydration: results from a microcrack model. J. Geophys. Res. 104, 10467–10481.

Strating, E., Vissers, R., 1991. Dehydration-induced fracturing of eclogite-facies peridotites. implications for the mechanical behavior of subducting oceanic lithosphere. Tectonophysics 200, 187–198.

Walder, J., Nur, A., 1984. Porosity reduction and pore pressure development. J. Geophys. Res. 89, 11539–11548.

Walther, J., Wood, B. (Eds.), 1986. Fluid–rock interactions during metamorphism. Advances in Physical Geochemistry. Springer-Verlag, New York.

Watt, G., Oliver, N., Griffen, B., 2000. Evidence for reaction-induced microfracturing in granulite facies migmatites. Geology 28, 327–330.

Wong, T.-F., Ko, S.-C., Olgaard, D., 1997. Generation and maintenance of pore pressure excess in a dehydrating system: 2. Theoretical analysis. J. Geophys. Res. 102, 841–852.